Article

Flexible Polyhedral Surfaces with Two Flat Poses

Hellmuth Stachel

Institute of Discrete Mathematics and Geometry, Vienna University of Technology, Wiedner Hauptstraße 8-10/104, 1040 Wien, Austria; E-Mail: stachel@dmg.tuwien.ac.at; Tel.: +431-58801-10434; Fax: +431-58801-10494

Academic Editor: Bernd Schulze

Abstract: We present three types of polyhedral surfaces, which are continuously flexible and have not only an initial pose, where all faces are coplanar, but pass during their self-motion through another pose with coplanar faces ("flat pose"). These surfaces are examples of so-called rigid origami, since we only admit exact flexions, *i.e.*, each face remains rigid during the motion; only the dihedral angles vary. We analyze the geometry behind Miura-ori and address Kokotsakis' example of a flexible tessellation with the particular case of a cyclic quadrangle. Finally, we recall Bricard's octahedra of Type 3 and their relation to strophoids.

1. Introduction

A polyhedral surface is called (continuously) flexible, when there is a continuous family of mutually incongruent poses, called flexions, sharing the intrinsic metric. Each face is a planar rigid body; only the dihedral angles can vary between faces sharing an edge.

In discrete differential geometry, but also in architecture, there is an interest in polyhedral structures that can change their shape while all faces remain rigid (see, e.g., [1]). Everybody can simulate this flexibility with real world models made from cardboard. However, one must be careful: the models of theoretically-rigid polyhedral surfaces can show a flexibility, due to imprecision and slight bending of the material. A famous example (see Figure 1) is described in Schwabe and Wunderlich's article [2] and was even exposed at the science exposition "Phänomena" 1984 in Zürich. At that time, it was falsely stated that this polyhedron is flexible. However, it is only snapping between two planar realizations and one spatial pose. The unfolding shows that all faces are congruent isosceles triangles.
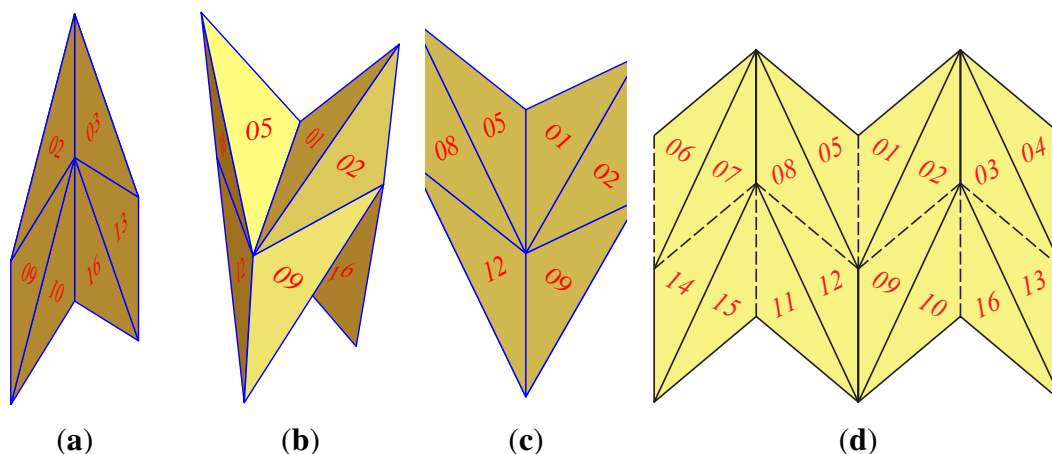
Figure 1. This polyhedron called "Vierhorn" is locally rigid, but snaps between its spatial pose (**b**) and the two flat realizations (**a**,**c**). Dashes in the unfolding (**d**) indicate valley folds.

Below, we present three examples of flexible polyhedral surfaces that share the property that they have (at least) two flexions where all faces are coplanar. Such poses will be called "flat".

- Firstly, we analyze the geometry behind Miura-ori.
- Secondly, we study Kokotsakis' flexible tessellation of convex quadrangles and a particular case with a second flat pose. These two examples include flexible 3×3-complexes of quadrangles, so-called quadrangular Kokotsakis meshes [3].
- Finally, we recall the well-known Bricard octahedra of Type 3. They can be characterized by having no global symmetry, and they admit two flat poses. We will emphasize the role of a particular cubic curve, the strophoid.

As a preparation, we provide a necessary condition for flexible polyhedral surfaces with two flat flexions. This condition refers to vertices V where four faces are meeting. Let α, β, γ and δ be the sequence of interior angles at V. Under the "vertex figure" of V, we understand the intersection of these four faces with a sphere, which is centered at V and whose radius is smaller than the shortest edge with endpoint V. Hence, the vertex figure is a spherical quadrangle with sides of lengths α, β, γ and δ (Figure 2). It has no effect on the flexions of this spherical quadrangle, when we replace any side of length λ by its complementary arc of length $2\pi - \lambda$. Therefore, we can confine ourselves to the case $\alpha, \ldots, \delta < \pi$; we call this quadrangle the reduced vertex figure.

Lemma 1. *Let a flexible polyhedral surface be given that passes through two flat poses. Then, at each vertex, where four faces are meeting, the reduced vertex figure has either a plane of symmetry, at least after replacing one or two vertices by their antipodes, or the sides coincide in pairs.*

Proof. The side lengths of the reduced vertex figure satisfy $0 < \alpha, \ldots, \delta < \pi$ (see Figure 2). The spherical quadrangle admits two aligned poses if two of the following four equations hold:

$$
\begin{aligned}
(a) \quad & \alpha + \beta + \gamma + \delta = 2\pi, & (c) \quad & \alpha - \beta + \gamma - \delta = 0, \\
(b) \quad & \alpha + \beta - \gamma - \delta = 0, & (d) \quad & \alpha - \beta - \gamma + \delta = 0
\end{aligned}
$$

It cannot happen that the length of one side, e.g., A_0B_0, equals the sum of the other three, since this spherical quadrangle admits only the aligned position. In any non-aligned pose of the polygon A_0ABB_0 with side lengths β, γ and δ, the distance between the initial point and the endpoint would be shorter than α. For a similar reason, a spherical quadrangle with $\beta + \gamma + \delta - \alpha = 2\pi$ cannot be continuously flexible.

Equations (a) and (b) are equivalent to $\beta = \pi - \alpha$ and $\delta = \pi - \gamma$. When we replace A and B by their respective antipodes $\overline{A}$ and $\overline{B}$, we obtain a spherical deltoid $A_0\overline{A}\,\overline{B}B_0$. The same holds in the case where (a) and (d) are satisfied. Replacing one vertex by its antipode means replacing one edge of the pyramid with apex V by its reflection with respect to V (note the extensions $\mathbf{P}_3^*$ and $\mathbf{P}_4^*$ of $\mathbf{P}_3$ and $\mathbf{P}_4$ in Figure 6).

Equations (a) and (c) are equivalent to $\gamma = \pi - \alpha$ and $\delta = \pi - \beta$. Then, the spherical quadrangle $A_0A\overline{B}B_0$ is an isogram, *i.e.*, a spherical quadrangle where opposite sides have the same length.

Equations (b) and (c) lead to $\alpha = \delta$ and $\beta = \gamma$, *i.e.*, to a spherical deltoid, as well as Equations (c) and (d). Equations (b) and (d) give a spherical isogram.

Spherical kites have either an axis of symmetry or the flexion is trivial, since the sides coincide in pairs. Spherical isograms are either self-intersecting with an axis of symmetry or they have a center of symmetry. When in the latter case two neighboring vertices are replaced by their antipodes, then the axial symmetry of the spherical isogram is transformed into a planar symmetry. □
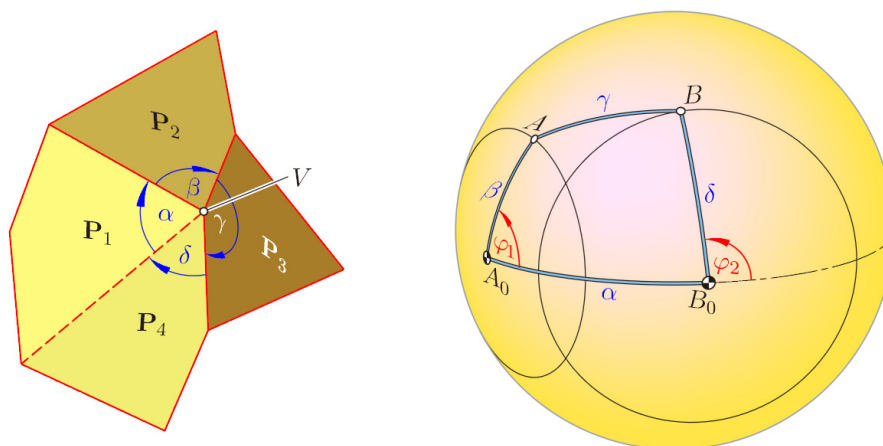
Figure 2. The interior angles at the vertex V serve as side lengths of the spherical four-bar A_0ABB_0, which controls the dihedral angles φ_1 and φ_2 during the flexion.

2. Miura-ori

Miura-ori is a Japanese folding technique named after Prof. Koryo Miura, The University of Tokyo. However, already before K. Miura, this technique was known; according to a personal communication with Gy. Darvas, it was kept as a military secret in Russia in the thirties of the last century. There are many applications of Miura-ori. It is, e.g., used for solar panels, because they can be packed in compact form and deployed into their flat shape by pulling on one corner only [4]. It serves as a kernel to stiffen sandwich structures. Furthermore, it can be utilized for the design of cupolas [1].

Let us analyze the process of folding a sheet of paper as depicted in Figure 3 with given valley and mountain folds, thus proving that this quadrangular surface is really continuously flexible. To begin with, we take two coplanar parallelograms with aligned upper and lower sides (Figure 4a).
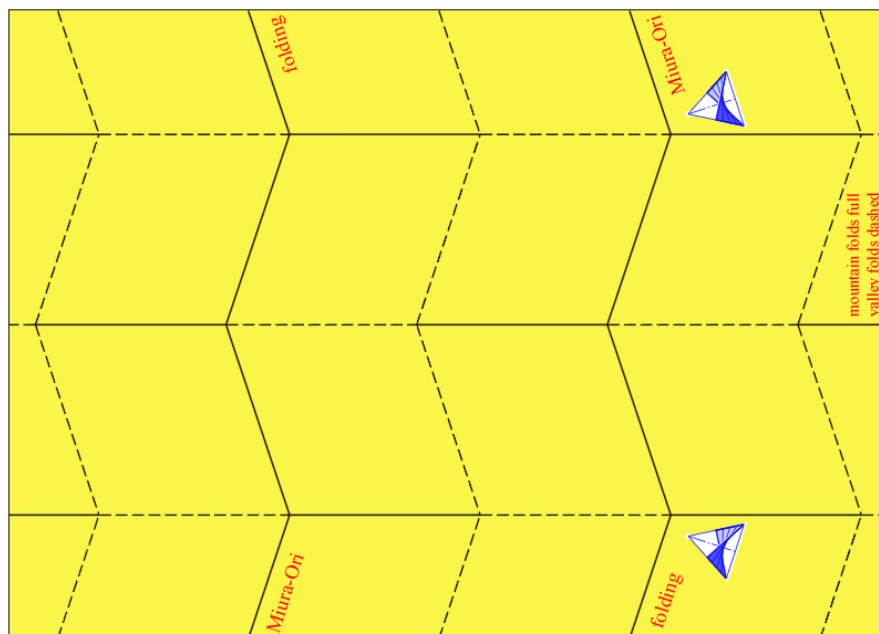
Figure 3. Miura-ori unfolded; dashes are valley folds; full lines are mountain folds.
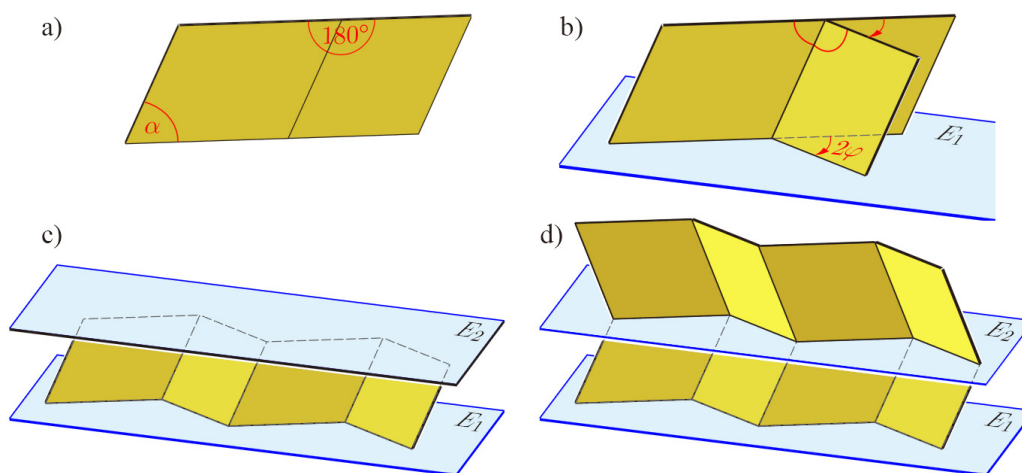
Figure 4. Generating neighboring zig-zag strips of Miura-ori.

Now, we rotate the parallelogram on the right-hand side against the left one about the common edge: the lower sides span a plane E_1, and the upper sides span a plane E_2 parallel to E_1. We continue and extend the two parallelograms to a zig-zag strip by adding parallelograms, which are translatory congruent alternately to the left-hand or right-hand parallelogram of the initial pair. After this, the complete strip has its lower zig-zag boundary still placed in E_1 and the upper one in E_2 (see Figure 4c). This remains valid when we fix the plane E_1, but vary the bending angle φ.

After iterated reflections in planes E_2 parallel to E_1 (Figure 4d) or after translations orthogonal to E_1, the complete Miura-ori flexion is obtained as depicted in (Figure 5). When finally the two initial parallelograms become coplanar due to a bending angle of 180°, Miura-ori reaches a totally folded pose, which is again flat.
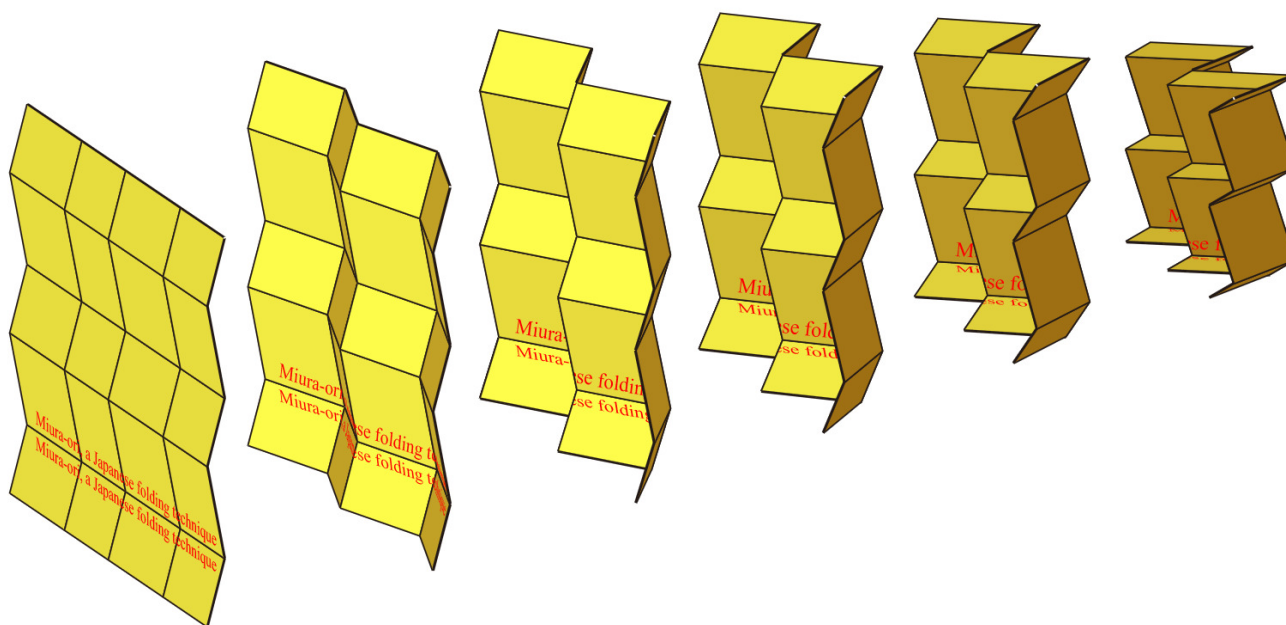
Figure 5. Snapshots of the folding procedure of Miura-ori.

The set of edges of Miura-ori can be subdivided into two families of folds. The "horizontal" folds are copies of the zig-zag line in E_1 and placed in horizontal planes. They are aligned in the stretched initial pose as depicted in Figure 3. The other folds are located in mutually parallel vertical planes, since their edges are obtained by iterated reflections in planes parallel to E_1. We call these folds "vertical". While the edges of each horizontal fold alternate between valley and mountain fold, all edges of a vertical fold are of the same type, either valley or mountain folds.

Now, we are going to analyze the self-motion of Miura-ori. For the sake of simplicity, we assume that all edges have a unit length (obviously, the side lengths of the zig-zag line in E_1 can vary without restricting the flexibility; analogously, the distances between the planes through the horizontal folds need not be the same everywhere).

We fix the planes of one horizontal and one vertical fold, as well as the crossing point V of these two folds (Figure 6). Let $\mathbf{P}_1, \ldots, \mathbf{P}_4$ be the four parallelograms meeting at V. We start with the motion of $\mathbf{P}_1$: the two edges of $\mathbf{P}_1$ with the common endpoint V rotate within the respective fixed planes, such that the included interior angle $\alpha < 90°$ remains constant (compare with Figure 4a). The reflection in the horizontal plane E_2 maps $\mathbf{P}_1$ onto the second parallelogram $\mathbf{P}_2$. It has the same interior angle α at V and moves like $\mathbf{P}_1$.

Now, we elongate the horizontal edges of the other two parallelograms $\mathbf{P}_3$ and $\mathbf{P}_4$ (with interior angle $180° - \alpha$) beyond the fixed vertical plane by the unit length. This gives two additional parallelograms $\mathbf{P}_3^*$ and $\mathbf{P}_4^*$ with the interior angle α at V. Each shares a "vertical" edge with $\mathbf{P}_1$ or $\mathbf{P}_2$, respectively. Hence, the reflection in the fixed vertical plane must map $\mathbf{P}_1$ onto $\mathbf{P}_3^*$ and $\mathbf{P}_2$ onto $\mathbf{P}_4^*$.

This reveals a hidden local symmetry of Miura-ori: when at each vertex V two adjacent parallelograms $\mathbf{P}_3$, $\mathbf{P}_4$ with congruent interior angles at V are replaced by their "horizontal elongations" $\mathbf{P}_3^*$ and $\mathbf{P}_4^*$, respectively, we obtain a pyramid of four congruent parallelograms $\mathbf{P}_1, \mathbf{P}_2, \mathbf{P}_3^*, \mathbf{P}_4^*$ with apex V. This pyramid flexes, such that it remains symmetrical with respect to the planes of the horizontal fold and the vertical fold passing through V (compare with Lemma 1).
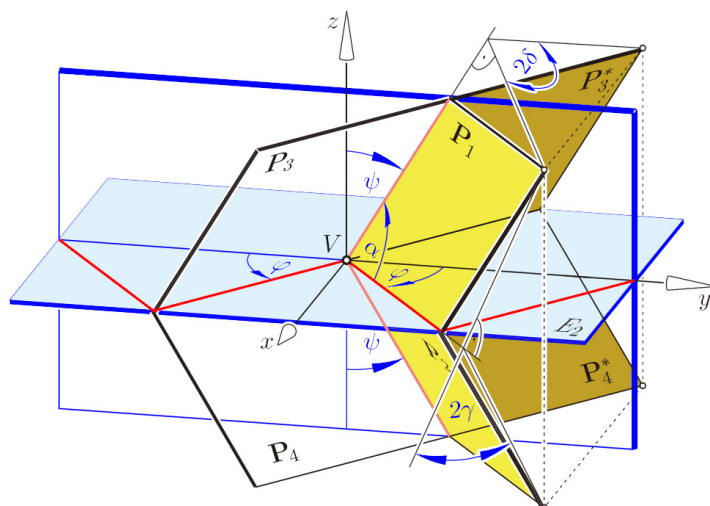
Figure 6. The two-fold local symmetry at each vertex V becomes visible when the edge between $\mathbf{P}_3$ and $\mathbf{P}_4$ is extended beyond V.

Next, we study the relations between angles: we use a coordinate frame with origin V, with the x- and y-axis in the horizontal plane E_2 and with the $[yz]$-plane spanned by the vertical fold passing through V (see Figure 6). Let 2φ and 2ψ be the bending angles between consecutive segments of the horizontal and vertical folds, respectively. Thus, the sides of $\mathbf{P}_1$ have the direction vectors:

$$\mathbf{h} = \begin{pmatrix} \sin\varphi \\ \cos\varphi \\ 0 \end{pmatrix}, \quad \mathbf{v} = \begin{pmatrix} 0 \\ \sin\psi \\ \cos\psi \end{pmatrix}$$

and we obtain the dot product:

$$\mathbf{h} \cdot \mathbf{v} = \cos\varphi \, \sin\psi = \cos\alpha = \text{const} \tag{1}$$

In the stretched position, the parallelogram $\mathbf{P}_1$ is located in the vertical $[yz]$-plane; the corresponding (half) bending angles are $\varphi = 0°$ and $\psi = 90° - \alpha$. The other limit is the totally folded position with $\mathbf{P}_1$ in the $[xy]$-plane, $\varphi = \alpha$ and $\psi = 90°$.

In order to obtain formulas for the dihedral bending angles 2γ and 2δ along edges of the horizontal and vertical folds (see Figure 6), we need the unit vector perpendicular to the plane of $\mathbf{P}_1$:

$$\mathbf{n} = \frac{1}{\sin\alpha}(\mathbf{h} \times \mathbf{v}) = \frac{1}{\sin\alpha} \begin{pmatrix} \cos\varphi \cos\psi \\ -\sin\varphi \cos\psi \\ \sin\varphi \sin\psi \end{pmatrix}$$

Its dot products with the unit vectors along the x- and z-axis give:

$$\cos\delta = \frac{\cos\varphi \, \cos\psi}{\sin\alpha}, \quad \sin\gamma = \frac{\sin\varphi \, \sin\psi}{\sin\alpha}, \quad 0 \leq \varphi \leq \alpha \tag{2}$$

Theorem 2. *During the self-motion of Miura-ori, the horizontal folds remain in mutually-parallel planes. The same holds for vertical folds, and their planes are orthogonal to the planes spanned by the horizontal folds. The dihedral bending angles 2γ along the edges of the horizontal folds are everywhere the same, as well as the angles 2γ for the vertical folds. They satisfy Equation (2), while φ and ψ are related by Equation (1).*

The motion depicted in Figures 4 and 5 is not the only self-motion of Miura-ori. The initial pose admits bifurcations. Trivial flexions arise, e.g., when in the stretched position, we use any aligned horizontal fold as an axis of rotation for a folding. The same can be done, independently of each other, with several aligned horizontal folds. Furthermore, after full $180°$-rotations, we obtain an n-fold covered strip and can treat it like a single strip. Hence, Miura-ori admits more than two flat poses.

Miura-ori is a very particular case of a Voss surface. This is a polyhedral surface with quadrangular faces, such that each 3×3 complex is a flexible Kokotsakis mesh [5] of the isogonal Type 3 (according to the enumeration given in [6]): at each vertex, opposite interior angles are either equal or complementary (Lemma 1); and there is an additional equation to satisfy ([7], p. 12). A long lasting open problem, the classification of flexible quadrangular Kokotsakis meshes [3] has recently been solved by I. Izmestiev [8]. The classification of flexible Kokotsakis meshes with a central n-gon and $n \geq 5$ is still open.

There are several generalizations of Miura-ori, among them the impressive approximations of free-form surfaces presented by T. Tachi in [9]. Some patterns are even examples of rigid origami [10], designed within the family of Voss surfaces.

3. Kokotsakis' Flexible Tessellation

Another remarkable flexible mesh of quadrangles, which also starts from a flat initial pose, dates back to A. Kokotsakis. In [5] (p. 647), he proved the flexibility of the tessellation displayed in Figure 7. However, he did not present any geometric property of its spatial poses; this will be done below.
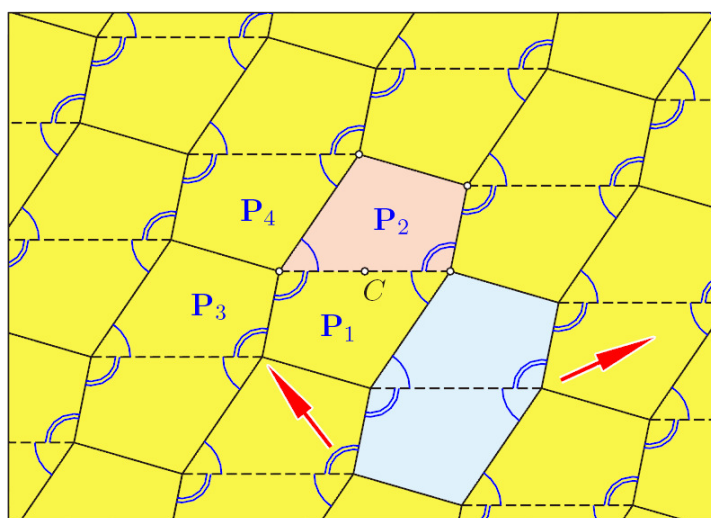
Figure 7. Kokotsakis' flexible mesh unfolded.

Choose an arbitrary quadrangle $\mathbf{P}_1$. By iterated rotations about the midpoints of the sides, we obtain a well-known regular tessellation of the plane (Figure 7). We can generate the same tessellation also in another way: when we glue together two adjacent quadrangles, we obtain a central-symmetric hexagon (blue shaded in Figure 7). Now, the same tessellation arises when this hexagon undergoes iterated translations, as indicated in Figure 7 by the red arrows.

In the following, we prove for convex quadrangles that this polyhedral structure is flexible: let $\mathbf{P}_1, \ldots, \mathbf{P}_4$ be four pairwise congruent faces with the common vertex V_1 (shaded area in Figure 8). They form a four-sided pyramid with apex V_1, and the four interior angles at V_1 are respectively congruent to the four interior angles of a quadrangle. Our pyramid is flexible, provided the fundamental quadrangle is convex; otherwise, one interior angle at V_1 would be greater than the sum of the other three interior angles, so that the only realization is flat.
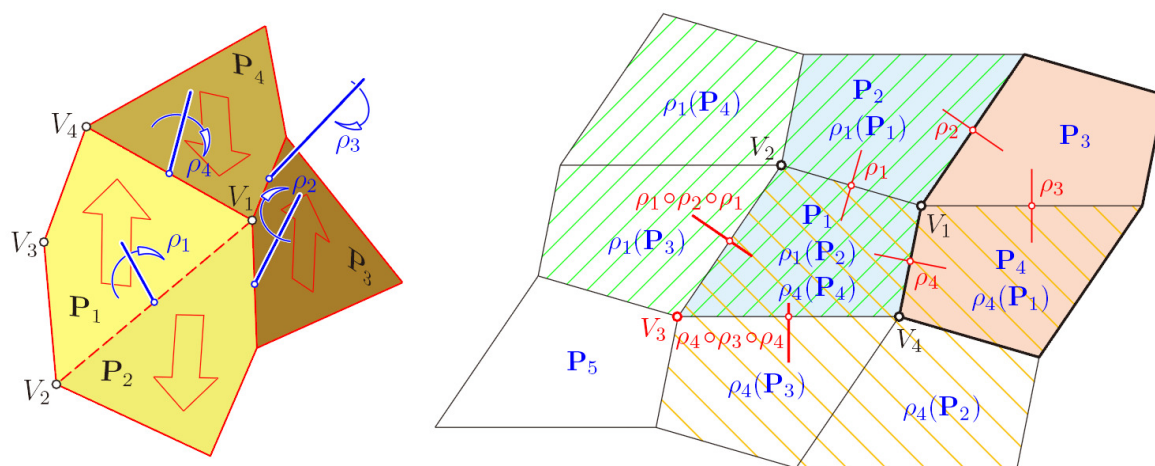
Figure 8. The flexion of a four-sided pyramid can be extended to a flexion of the complete tessellation.

According to the labeling in Figure 8, left, for any pair of adjacent faces, there is a respective 180°-rotation ("half-turn") ρ_1, ρ_2, ρ_3 or ρ_4, which exchanges the two faces. Therefore, e.g., $\mathbf{P}_2 = \rho_1(\mathbf{P}_1)$. The axis of ρ_1 is perpendicular to the common edge $V_1 V_2$ and located in a plane that bisects the dihedral angle between $\mathbf{P}_1$ and $\mathbf{P}_2$.

After applying consecutively all four half-turns to the quadrangle $\mathbf{P}_1$, this is mapped via $\mathbf{P}_2$, $\mathbf{P}_3$ and $\mathbf{P}_4$ onto itself. This implies:

$$\rho_4 \circ \rho_3 \circ \rho_2 \circ \rho_1 = \mathrm{id}\,, \quad \text{hence} \quad \rho_1 \circ \rho_2 = \rho_4 \circ \rho_3 \tag{3}$$

Now, we can extend this flexion of the pyramid step by step to the complete tessellation: the rotation ρ_1 exchanges not only $\mathbf{P}_1$ with $\mathbf{P}_2$, but transforms the pyramid with apex V_1 onto a congruent copy with apex V_2 sharing two faces with its preimage. This is the area hatched in green in Figure 8, right. Analogously, ρ_4 generates a pyramid with apex V_4 sharing the faces $\mathbf{P}_1$ and $\mathbf{P}_4$ with the initial pyramid. Finally, there are two ways to generate a pyramid with apex V_3. Either we transform ρ_2 by ρ_1 and apply $\rho_1 \circ \rho_2 \circ \rho_1$, which exchanges V_2 with V_3, or we proceed with $\rho_4 \circ \rho_3 \circ \rho_4$, which exchanges V_4 with V_3. Thus, we obtain two mappings, $\rho_1 \circ \rho_2$ and $\rho_4 \circ \rho_3$, with $V_1 \mapsto V_3$, which are equal by virtue of

Equation (3). Hence, each flexion of the initial pyramid with apex V_1 is compatible with a flexion of the 3×3 complex of quadrangles. This can be extended to the complete tessellation (in [6], it is shown that this tessellation is a particular case of the line-symmetric Type 5 of flexible Kokotsakis meshes).

The product of two half-turns is a helical motion about the common perpendicular of the axes of the two half-turns. The angle of rotation and the length of translation is twice the angle and distance, respectively, between the two axes. When the pyramid with apex V_1 is not flat, then the axes of the $180°$-rotations $\rho_1, \ldots, \rho_4$ are pairwise skewed; the common perpendicular of any two of them is unique. Equation (3) implies that the axes of the four rotations have a common perpendicular a. Hence, the motions $\rho_1 \circ \rho_2$ and $\rho_3 \circ \rho_2 = \rho_4 \circ \rho_1$ are helical motions with a common axis a. All vertices of the flexion have the same distance to a; they lie on a cylinder Ψ or revolution (in [11], T. Tarnai addresses another relation between planar tessellations and cylindrical shapes; he shows how semiregular tessellations can be folded into cylindrical shells).

When the quadrangles $\mathbf{P}_3$ and $\mathbf{P}_4$ are glued together, we obtain a line-symmetric skewed hexagon, one half of our initial pyramid with apex V_1; the half-turn ρ_3 maps this hexagon onto itself (Figure 8). We can generate the complete flexion by applying iterated helical motions $\rho_1 \circ \rho_2$ and $\rho_3 \circ \rho_2$ on this hexagon.

Theorem 3. *Any flexion of the Kokotsakis tessellation is obtained from the line-symmetric hexagon consisting of the two planar quadrangles by applying the discrete group of coaxial helical motions generated by $\rho_1 \circ \rho_2$ and $\rho_3 \circ \rho_2$. In the initial flat pose, these generating motions are the translations applied to a centrally symmetric hexagon, thus generating the regular tessellation in the plane.*

The flat initial pose of the pyramid with apex V_1 admits a bifurcation between two continuous motions of the pyramid. Hence, the complete quad mesh admits two self-motions (Figure 9). When starting with a trapezoid $\mathbf{P}_1$ (compare with Figure 14 in [12]), one of these self-motions is trivial: it results from mutually-independent bending along aligned edges of the initial pose.
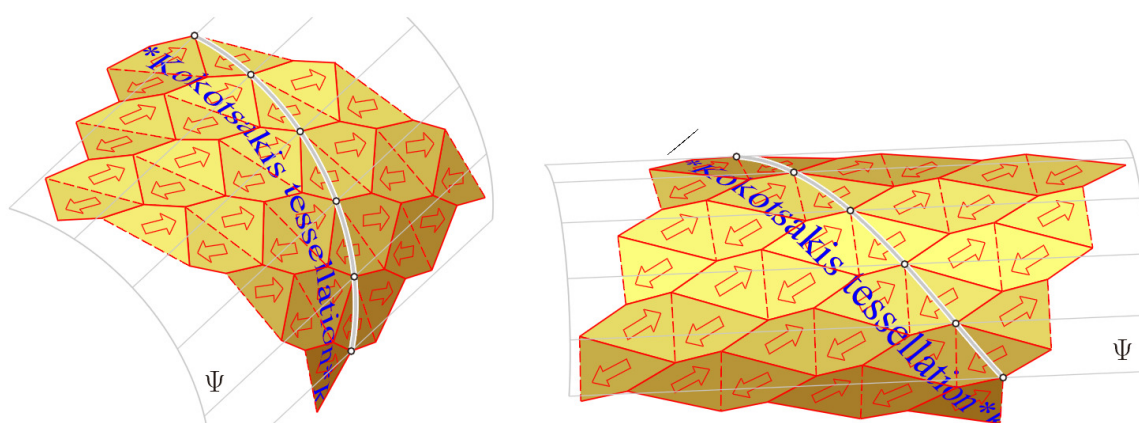
Figure 9. The Kokotsakis tessellation admits two self-motions.

Once we have clarified that for each non-planar flexion, all vertices lie on a cylinder Ψ of revolution with axis a, we can give another explanation for the flexibility (see Figure 10): the plane spanned by the quadrangle $V_1 \ldots V_4$ intersects the circumcylinder Ψ along an ellipse $\mathcal{E}$. Given a convex quadrangle $V_1 \ldots V_4$, there is a pencil of conics passing through the four vertices. This pencil includes an infinite set

of ellipses, which is bounded by parabolas or pairs of parallel lines. Hence, we can specify an ellipse $\mathcal{E}$ out of this pencil and choose one of the two right cylinders passing through $\mathcal{E}$.

Now, we define the half-turns ρ_1 and ρ_4; their axes pass through the midpoints of the sides V_1V_2 and V_1V_4, respectively, and intersect the cylinder's axis a perpendicularly (see Figure 10). The common normal of the lines V_2V_3 and a is the axis of $\rho_1 \circ \rho_2 \circ \rho_1$; that between V_3V_4 and a is the axis of $\rho_4 \circ \rho_3 \circ \rho_4$. Iterations of these half-turns transform our initial face $\mathbf{P}_1$ into all faces of the flexion.
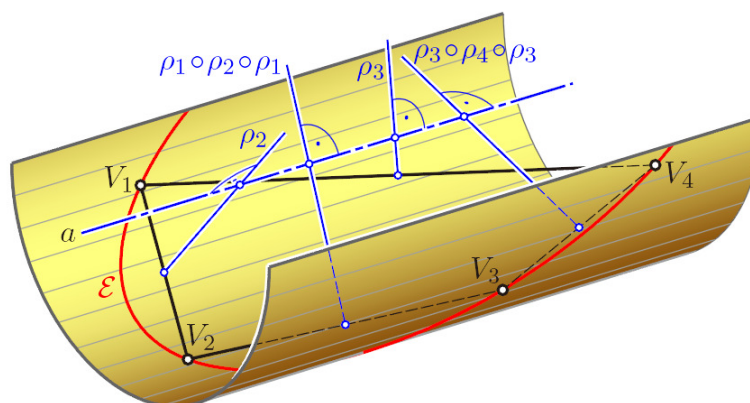
Figure 10. There is an infinite set of ellipses passing through the vertices of a convex quadrangle.

In [12], cases are studied where a particular flexion of a $m \times n$-complex closes. This gives rise to an infinitesimally rigid tessellation on a right cylinder by plane quadrangles (see Figure 11).
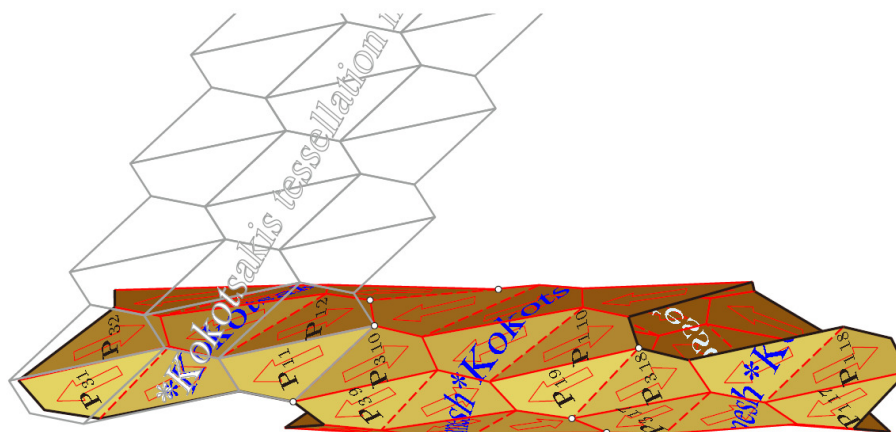
Figure 11. This is an infinitesimally rigid pose of a flexible tessellation mesh [12].

Theorem 4. *When the basic quadrangle of the flexible Kokotsakis' tessellation is cyclic, i.e., has a circumcircle, it admits a second flat pose: all quadrangles are packed into a single circumcircle. However, this fails for real-world models, because of self-intersections.*

Proof. In the case of a cyclic quadrangle, the pencil of circumscribed conics includes one circle. There is a unique right cylinder passing through this circle, and the corresponding axes of half-turns $\rho_1, \ldots, \rho_4$ are coplanar. The complete flexion is flat; the circumcircles of all faces coincide (compare with Figure 12).

Similar to Miura-ori, this tessellation mesh can be "packed" into a very small size, such that it finds a place in the circumcircle of one quadrangle, at least "theoretically", *i.e.*, without paying attention to self-intersections. However, a real-world model consisting of at least 3×3 quadrangles cannot approach such a pose, since the faces have to be placed one upon the other. Then, there is a collision between the "edges" spanning over distant levels and the vertices of quadrangles placed between them.   □
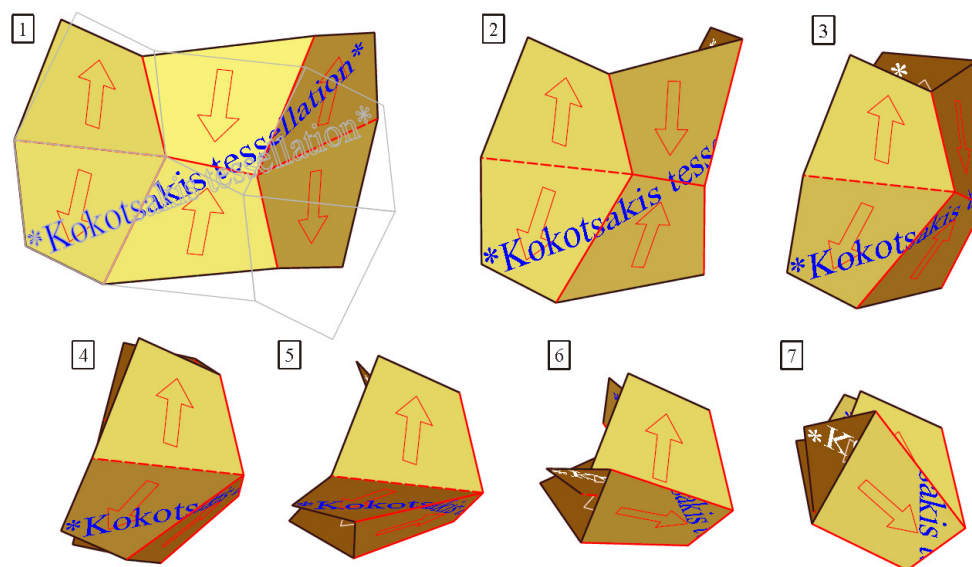
Figure 12. The tessellation mesh of a cyclic quadrangle admits a second flat pose.

In the case of a cyclic quadrangle, opposite angles are complementary. Therefore, this flexible tessellation is an example of a Voss surface, too.

4. Bricards' Octahedra of Type 3

In this final section, an octahedron is understood as a double-pyramid over a quadrangle, which need not be planar. Hence, the octahedron contains three pairs (A, A'), (B, B') and (C, C') of opposite vertices. Each of them can be seen as a pair of apices of a double pyramid; the corresponding bases, called "equators", are the quadrangles $BCB'C'$, $ACA'C'$ or $ABA'B'$, respectively.

According to R. Bricard's fundamental result [13], there are three types of flexible octahedra. Those without any symmetry belong to Type 3 and admit two flat poses. They can be defined as shown in Figure 13a.

Each of the three equators is a quadrangle with sides tangent to a circle with the same center M. Hence, there is a local symmetry at each vertex with respect to an axis, which passes through M (note Lemma 1).

The following theorem relates the given flat pose to a strophoid $\mathcal{S}$, which is defined as a circular curve of degree three with a node N and orthogonal tangents at the node. On $\mathcal{S}$, a symmetric relation can be defined [14]: two points P, P' of $\mathcal{S} \setminus \{N\}$ are called associated if the lines NP and NP' are symmetric with respect to the node tangents t_1 and t_2. Furthermore, the strophoid $\mathcal{S}$ is the locus of points X with the property that one angle bisector of the lines XP and XP' passes through the node N. This holds simultaneously for all pairs (P, P') of associated points of $\mathcal{S}$.

As a consequence, at our given flat pose of the octahedron, there must be a strophoid $\mathcal{S}$ with the node $N = M$ and associated points (A, A'), such that $\mathcal{S}$ passes also through B, B', C and C' (Figure 13b).
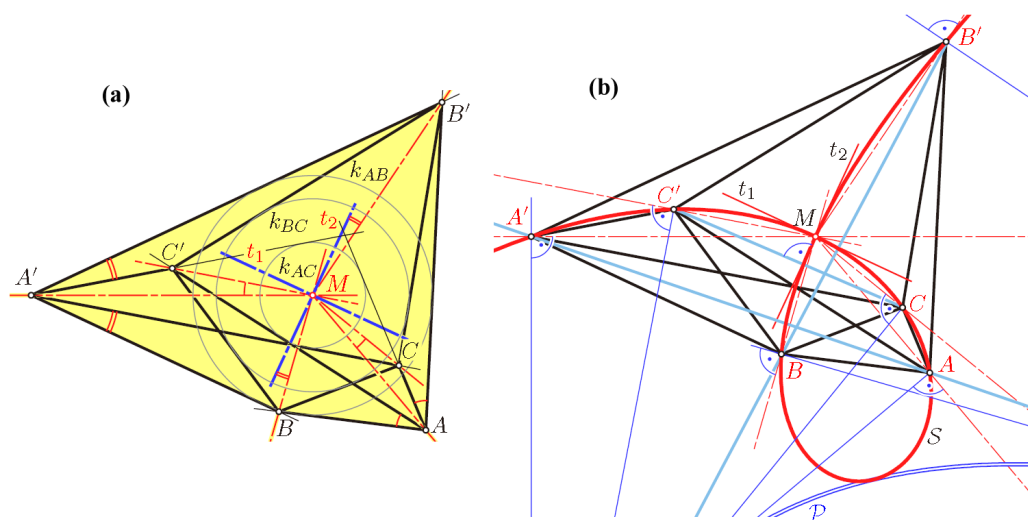
Figure 13. In the flat pose, the pairs of opposite points of Bricard's Type-3 flexible octahedron are associated with a strophoid $\mathcal{S}$.

Theorem 5. *For any strophoid $\mathcal{S}$, each triple of associated pairs of points (A, A'), (B, B') and (C, C') defines a flat pose of a flexible octahedron. This octahedron has a second flat pose.*

Proof. In order to obtain the second flat pose, let us keep the face ABC fixed, while the opposite triangle $A'B'C'$ is replaced by a congruent copy $A''B''C''$. Both flat poses must show respectively equal distances $AB' = AB''$, $AC' = AC''$, ..., $CB' = CB''$. We show that the reflection in the line AB maps C' onto C'', the reflection in the line AC maps B' onto B'' and the reflection in the line BC maps A' onto A'' (see Figure 14). Firstly, these reflections preserve the distances to the points of the fixed triangle. Secondly, since both pairs of lines, (AB, AB') and (AC, AC'), are symmetric with respect to AM, the angles $\sphericalangle B'AB'' = 2 \sphericalangle B'AC$ and $\sphericalangle C'AC'' = 2 \sphericalangle C'AB$ are equal. Hence, there is a rotation about A, which sends the side $B'C'$ onto $B''C''$ and preserves the length. The same holds for the other sides $A'B'$ and $A'C'$. $\square$

Furthermore, at spatial poses of the flexible octahedron of Type 3, there is a local symmetry at each vertex V (Lemma 1): the six planes of symmetry share a common axis a (see, e.g., [15], Figure 3). All equators are placed on one-sheet hyperboloids of revolution with the axis a. As demonstrated in [16,17], even at each spatial pose, there is a particular spatial cubic passing through the six vertices. Of course, this cubic is the spatial analogue of the strophoid $\mathcal{S}$ displayed in Figure 13b.

All flexible octahedra have self-intersections. Real-world models work only when either they are built as a framework or one pair of opposite faces is removed (see, e.g., [7], Figure 5).

There exist also particular flexible octahedra of Type 2, *i.e.*, with an axis of symmetry, which admit two flat poses. They are a sort of limiting case when point M in Figure 13a, tends to infinity (see, e.g., [15], Figure 4). G. Nawratil [18] proved that there is one non-trivial type of a flexible octahedron with some vertices at infinity: it consists of two prisms with a kite as the common basis; the generators

of the prisms are orthogonal to the kite's axis of symmetry. These examples can even be free of self-intersections.

The analogue of Type 3 in the hyperbolic space is also flexible. Of course, more sub-types can be distinguished, since the vertices can be either finite points or on the absolute conic or outside (note [19]). Recently, A.A. Gaifullin generalized all of this in [20]: He proved that, in the algebraic sense, Type 3 is the simplest; there exist flexible higher-dimensional analogues, so-called cross-polytopes, in all dimensions, in Euclidean spaces, as well as in spherical and hyperbolic spaces.
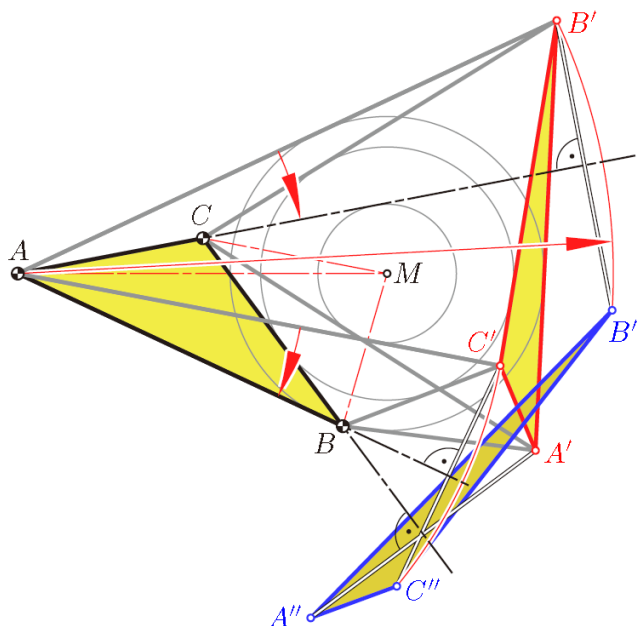
Figure 14. The two flat poses of a Type-3 flexible octahedron.

5. Conclusions

This paper focuses on three well-known examples of continuously-flexible polyhedral surfaces and analyzes the geometry behind them. Emphasis is placed on versions with two flat poses. The examples, which are studied in detail, are Miura-ori, A. Kokotsakis' flexible tessellation with congruent convex quadrangles and R. Bricard's Type-3 octahedra. We do not claim that the presented three examples are the only ones with two flat poses.

Conflicts of Interest

The author declares no conflict of interest.

References and Notes

1. Barej, M.; Hoffmann, S.; Knief, Ch.; Trautz, M.; Corves, B. Design and Application Studies for a Cupola Forming Orbital Arrangment of Miura-Ori Basic Units. *J. Geom. Graph.* **2015**, *19*, in press.

2. Wunderlich, W.; Schwabe, C. Eine Familie von geschlossenen gleichflächigen Polyedern, die fast beweglich sind. *Elem. Math.* **1986**, *41*, 88–98.

3. A *Kokotsakis mesh* is a polyhedral structure consisting of an n-sided central polygon $\mathbf{P}_0$, $n \geq 3$, which is surrounded by a belt of other polygons; at each vertex of $\mathbf{P}_0$ four faces are meeting [5]. In the case $n = 4$ the mesh is called *quadrangular*. The *triangular case* $(n = 3)$ is equivalent to an octahedron.

4. Miura, K. *Method of Packaging and Deployment of Large Membranes in Space*; Report No. 618; The Institute of Space and Astronautical Science: Tokyo, Japan, 1985.

5. Kokotsakis, A. Über bewegliche Polyeder. *Math. Ann.* **1932**, *107*, 627–647.

6. Stachel, H. A kinematic approach to Kokotsakis meshes. *Comput. Aided Geom. Des.* **2010**, *27*, 428–437.

7. Stachel, H. On the flexibility and symmetry of overconstrained mechanisms. *Philos. Trans. A Math. Phys. Eng. Sci.* **2013**, *372*, doi:10.1098/rsta.2012.0040.

8. Izmestiev, I. *Classification of Flexible Kokotsakis Polyhedra with Quadrangular Base*; Cornell University Library: Ithaca, NY, USA, 2014; p. 76.

9. Tachi, T. Freeform Variations of Origami. *J. Geom. Graph.* **2010**, *14*, 203–215.

10. Tachi, T. Generalization of Rigid Foldable Quadrilateral Mesh Origami. *J. IASS* **2009**, *50*, 173–179.

11. Tarnai, T. Folding of Uniform Plane Tessellations. In Proceedings of the 2nd International Meeting of Origami Science and Scientific Origami, Otsu/Shiga, Japan, 29 November–2 December 1994; pp. 83–91.

12. Stachel, H. A Flexible Planar Tessellation with a Flexion Tiling a Cylinder of Revolution. *J. Geom. Graph.* **2012**, *16*, 153–170.

13. Bricard, R. Mémoire sur la théorie de l'octaèdre articulé. *J. Math. Pur. Appl. Liouville* **1897**, *3*, 113–148. (In French)

14. Abu-Saymeh, S.; Hajja, M.; Stachel, H. Equicevian Points and Cubics of a Triangle. *J. Geom. Graph.* **2014**, *18*, 133–157.

15. Stachel H. Zur Einzigkeit der Bricardschen Oktaeder. *J. Geom.* **1987**, *28*, 41–56.

16. Bricard, R. *Leçons de Cinématique*; Gauthier-Villars: Paris, France, 1926; Tome I. (In French)

17. Bricard, R. *Leçons de Cinématique*; Gauthier-Villars: Paris, France, 1927; Tome II. (In French)

18. Nawratil, G. Flexible octahedra in the projective extension of the Euclidean 3-space. *J. Geom. Graph.* **2010**, *14*, 147–169.

19. Slutskiy, D. A necessary flexibility condition of a nondegenerate suspension in Lobachevsky 3-space. *Russ. Acad. Sci. Sb. Math.* **2012**, doi:10.1070/SM2013v204n08ABEH004336.

20. Gaifullin, A.A. Flexible Cross-Polytopes in Spaces of Constant Curvature. *Proc. Steklov Inst. Math.* **2014**, *286*, 77–113.